Discovery of Acetylcholinesterase Peripheral Anionic Site Ligands through Computational Refinement of a Directed Library†

Tobin J. Dickerson,‡ Albert E. Beuscher IV,§ Claude J. Rogers,‡ Mark S. Hixon,‡ Noboru Yamamoto,‡ Yang Xu,‡ Arthur J. Olson,§ and Kim D. Janda*,‡

Departments of Chemistry, Immunology, and Molecular Biology and The Skaggs Institute for Chemical Biology, The Scripps Research Institute, 10550 North Torrey Pines Road, La Jolla, California 92037

Received August 12, 2005; Revised Manuscript Received September 15, 2005

ABSTRACT: The formation of β-amyloid plaques in the brain is a key neurodegenerative event in Alzheimer's disease. Small molecules capable of binding to the peripheral anionic site of acetylcholinesterase (AChE) have been shown to inhibit the AChE-induced aggregation of the β-amyloid peptide. Using the combination of a computational docking model and experimental screening, five compounds that completely blocked the amyloidogenic effect of AChE were rapidly identified from an ∼200-member library of compounds designed to disrupt protein−protein interactions. Critical to this docking model was the inclusion of two explicit water molecules that are tightly bound to the enzyme. Interestingly, none of the tested compounds inhibited the related enzyme butyrylcholinesterase (BuChE) up to their aqueous solubility limits. These compounds are among the most potent inhibitors of amyloid β-peptide aggregation and are equivalent only to propidium, a well-characterized AChE peripheral anionic site binder and aggregation inhibitor.

Alzheimer's disease (AD)[1] is the leading cause of dementia and the most common amyloidosis of the brain (*1*, *2*). One of the primary neuropathological hallmarks of AD is deposition of the β-amyloid peptide (Aβ) into amyloid plaques in areas of the brain important for memory and cognition (*3*). Currently, approximately 6−8% of all individuals over the age of 65 have AD, and the prevalence doubles for every 5 years after age 60 (*1*). With AD cases expected to triple over the next half-century (*4*), the development of treatments that slow or halt the disease progression have become imperative to both improve the quality of life for patients and caregivers as well as drastically reduce the health care costs attributable to the disease.

Although extensive study into AD has been performed, the precise mechanism leading to the onset of the disease remains unclear. Self-assembly of Aβ, a naturally occurring soluble protein, into oligomers and fibrils has been linked to the compromise of neuronal function. The fact that diffuse plaques, while more numerous, evoked little neuronal loss or reactive gliosis, combined with the observation that compacted plaques composed of fibrillar Aβ are often associated with neuronal loss, dystrophic neuritis, as well as reactive astrocytes and activated microglia, has given rise to the hypothesis that fibril formation by Aβ starts an "amyloid cascade" composed of inflammatory and oxidative stress responses that eventually leads to neuron loss (*5*−*9*). Therapies designed to modulate the aggregation of Aβ may contribute to delaying the progression of AD as recent data indicates that Aβ changes occur earlier in the AD disease process than the formation of neurofibrillary tangles, another neuropathological structure used to characterize AD severity (*10*).

Recent studies have revealed that Aβ can selectively interact with various molecules that affect folding and aggregation of the peptide (*11*). In particular, acetylcholinesterase (AChE) has been identified as a target for AD therapy as the formation of stable complexes between the enzyme and Aβ has been implicated as accelerators of fibril formation (*12*). The mechanism of this proaggregating phenomenon is speculated to result from an activity of the enzyme not directly related to its catalytic function; specifically, interactions between the entrance of the binding site gorge, possibly interacting with the peripheral anionic binding site (PAS), and Aβ have been proposed to lead to increased fibril formation (*13*). Support for this hypothesis was given by studies demonstrating that while active site inhibitors do not reduce Aβ aggregation, the PAS-specific compound propidium was able to abrogate fibril formation (*13*, *14*). In this context, a resurgence in the identification of AChE inhibitors has occurred in an effort to find new molecules capable of interacting with the AChE peripheral anionic site for use as possible therapeutics to treat AD (*15*−*17*). Additionally, dual function inhibitors that can both

† This work was supported financially by The Scripps Research Institute and The Skaggs Institute for Chemical Biology.

* Corresponding author. Phone: 858-784-2516. Fax: 858-784-2595. E-mail: kdjanda@scripps.edu.

‡ Departments of Chemistry and Immunology and The Skaggs Institute for Chemical Biology.

§ Department of Molecular Biology.

[1] Abbreviations: 4CC, four-component condensation; Aβ, β-amyloid peptide; AChE, acetylcholinesterase; AcOH, acetic acid; AD, Alzheimer's disease; ATCh, acetylthiocholine; BuChE, butyrylcholinesterase; Boc, *tert*-butoxycarbonyl; DMF, *N*,*N*-dimethylformamide; DMSO, dimethyl sulfoxide; DTNB, 5,5′-dithiobis(2-nitrobenzoic acid); ESI-TOF, electrospray ionization time of flight; EtOAc, ethyl acetate; HRMS, high-resolution mass spectrometry; HuAChE, human acetylcholinesterase; mAChE, murine acetylcholinesterase; MeOH, methanol; NMR, nuclear magnetic resonance; PAS, peripheral anionic binding site; RMS, root mean square; RMSD, root mean square deviation; TLC, thin-layer chromatography.

10.1021/bi051613x CCC: $30.25
Published on Web 10/21/2005

inhibit AChE while also interacting with the PAS have also been studied as an approach to address the cholinergic deficits associated with AD while also inhibiting Aβ aggregation (*13*, *14*).

We have recently begun to explore the ability of what we have termed "credit card" libraries to inhibit protein−protein interactions relevant to various diseases (*18*). Specifically, these libraries are based upon flat, rigid scaffolds that can be rapidly synthesized and yet provide adequate diversity to impart protein specificity. The underlying concept behind the design of these libraries stems from the recognition that protein−protein interactions are predominantly comprised of aromatic, shallow depressions typically different from the deep binding clefts generally found in proteins. Thus, binding of the correct "card" translates into a disruption of the desired protein−protein interaction. Herein, we report the tandem computational and experimental identification of compounds from a credit card library that inhibit acetylcholinesterase (AChE) and reduce the ability of the β-amyloid peptide to aggregate and form fibrils.

EXPERIMENTAL PROCEDURES

General Synthetic Procedures. The ^{1}H NMR and ^{13}C NMR spectra were recorded on a Bruker DRX-600 or Varian INOVA-400 instrument, unless otherwise noted. High-resolution mass spectra (HRMS) were recorded at The Scripps Research Institute on an Agilent mass spectrometer using electrospray ionization (ESI-TOF). All reactions were monitored by thin-layer chromatography (TLC) carried out on 0.25 mm E. Merck silica gel plates (60F-254), with fractions being visualized by UV light. Methylene chloride and chloroform were distilled from calcium hydride. Tetrahydrofuran (THF) was distilled from sodium/benzophenone. Methanol was distilled from magnesium. Reagents were purchased at the highest commercial quality and used without further purification. All reactions were carried out under an argon atmosphere, unless otherwise noted. Reported yields were determined after purification to a homogeneous material.

6-(Benzyloxy)-2-naphthaldehyde and 6-(4-Methoxybenzyloxy)-2-naphthaldehyde. To a stirring solution of 6-hydroxy-2-naphthaldehyde (1.00 g, 5.8 mmol) and K_2CO_3 (4.0 g, 29 mmol) in DMF (30 mL) was added either benzyl chloride (810 mg, 6.4 mmol) or 4-methoxybenzyl chloride (0.87 mL, 6.4 mmol), and the solution was stirred at 80 °C. After 2 h, the mixture was diluted with EtOAc (200 mL) and water (300 mL). The phases were separated, and the aqueous layer was washed with EtOAc (200 mL). The combined organics were washed with water and then brine and dried over $MgSO_4$. Filtration, followed by concentration in vacuo, returned the product as a white solid, which was used without further purification.

*6-(Benzyloxy)-2-naphthaldehyde (**2a**):* ^{1}H NMR (500 MHz, $CDCl_3$) δ 10.10 (s, 1H), 8.26 (s, 1H), 7.91 (m, 2H), 7.80 (d, J = 8.5 Hz, 1H), 7.42 (d, J = 8.5 Hz, 2H), 7.29 (m, 2H), 6.95 (d, J = 8.5 Hz, 2H), 5.15 (s, 2H), 3.83 (s, 3H). ^{13}C NMR (125 MHz, $CDCl_3$) δ 192.0, 167.6, 160.1, 159.9, 138.6, 134.7, 132.8, 131.6, 128.7, 128.2, 124.1, 120.7, 107.8, 70.5, 55.8.

*6-(4-Methoxybenzyloxy)-2-naphthaldehyde (**2b**):* ^{1}H NMR (500 MHz, $CDCl_3$) δ 10.10 (s, 1H), 8.27 (s, 1H), 7.92 (m, 2H), 7.80 (d, J = 8.5 Hz, 1H), 7.50 (d, J = 7 Hz, 2H), 7.43 (t, J = 7 Hz, 2H), 7.34 (m, 1H), 7.32 (dd, J = 2.5, 9 Hz, 1H), 7.28 (d, J = 2.5 Hz, 1H), 5.22 (s, 2H).

General Procedure for Ugi Four-Component Condensations. To a solution of naphthal derivative **2** (0.2 mmol, 1.0 equiv) in MeOH were added acid (0.4 mmol, 2.0 equiv), amine (0.4 mmol, 2.0 equiv), and isocyanide (0.4 mmol, 2.0 equiv). After being stirred for 24 h at reflux, the mixture was cooled to room temperature and concentrated in vacuo. The residue was purified by a short silica gel column packed in a 5 mL Teflon syringe with a 10−50% EtOAc/hexane gradient to afford the desired product. All products were analyzed by ^{1}H NMR and HRMS.

*N-Cyclohexyl-2-{(4-methoxybenzyl)-[2-(4-methoxyphenyl)-acetyl]amino}-2-[6-(4-methoxybenzyloxy)naphthalen-2-yl]-acetamide (**3**):* ^{1}H NMR (500 MHz, $CDCl_3$) δ 7.71 (s, 1H), 7.61 (m, 2H), 7.39 (m, 3H), 7.15 (m, 4H), 6.94 (d, J = 8.5 Hz, 4H), 6.86 (m, 2H), 6.68 (d, J = 8 Hz, 2H), 5.95 (br s, 0.9H), 5.77 (br d, J = 6 Hz, 1.1H), 5.09 (s, 2H), 4.69 (br d, J = 17 Hz, 0.8H), 4.59 (d, J = 25 Hz, 0.2H), 4.48 (br d, J = 17 Hz, 0.8 H), 4.33 (d, J = 5.5 Hz, 0.2H), 3.83 (s, 3H), 3.81 (s, 1H), 3.78 (s, 3H), 3.71 (s, 3H), 3.63 (dd, J = 14.5, 21.5 Hz, 2 H), 3.57 (s, 0.8H), 3.56 (s, 0.2H), 1.88 (m, 2H), 1.59 (m, 3H), 1.31 (m, 2H), 1.06 (m, 3H). ^{13}C NMR (125 MHz, $CDCl_3$) δ 175.7, 173.7, 169.1, 160.0, 159.2, 159.1, 158.9, 157.8, 134.6, 131.0, 130.8, 130.4, 130.0, 129.7, 129.3, 129.1, 127.9, 127.7, 127.2, 126.2, 120.0, 114.9, 114.8, 114.6, 114.5, 114.4, 114.3, 107.3, 70.3, 63.8, 55.7, 55.6, 50.3, 49.0, 43.5, 43.3, 41.0, 40.4, 33.2, 25.9, 25.2. ESI-TOF calcd for $C_{43}H_{46}N_2O_6$ [M + H$^+$] 687.3428, found 687.3415.

*2-{Butyl[2-(4-methoxyphenyl)acetyl]amino}-N-cyclohexyl-2-[6-(4-methoxybenzyloxy)naphthalen-2-yl]acetamide (**4**):* ^{1}H NMR (600 MHz, $CDCl_3$) δ 7.79 (s, 1H), 7.69 (d, J = 8.5 Hz, 2H), 7.40 (m, 3H), 7.21 (m, 5H), 6.94 (d, J = 8 Hz, 2H), 6.86 (d, J = 8 Hz, 2H), 6.02 (br s, 0.9H), 5.96 (s, 1.1H), 5.10 (s, 2H), 3.82 (s, 3H), 3.80 (m, 4H), 3.71 (dd, J = 14.5, 21.5 Hz, 2H), 3.34 (m, 2H), 1.89 (m, 2H), 1.64 (m, 2H), 1.57 (m, 1H), 1.46 (m, 1H), 1.34 (m, 2H), 1.05 (m, 6H), 0.68 (t, J = 7 Hz, 3H). ^{13}C NMR (150 MHz, $CDCl_3$) δ 172.3, 168.9, 159.5, 158.5, 157.3, 134.1, 130.6, 130.5, 129.9, 129.6, 129.3, 128.6, 128.3, 127.4, 127.1, 127.0, 119.6, 114.3, 114.0, 113.8, 106.8, 69.8, 64.9, 62.7, 60.3, 55.3, 55.2, 48.4, 47.1, 40.0, 32.7, 31.8, 31.5, 25.4, 24.7, 21.0, 20.0, 14.1, 13.7, 13.4. ESI-TOF calcd for $C_{39}H_{46}N_2O_5$ [M + H$^+$] 623.3479, found 623.3460.

*N-Benzyl-2-{(4-methoxybenzyl)-[2-(4-methoxyphenyl)acetyl]-amino}-2-[6-(4-methoxybenzyloxy)naphthalen-2-yl]acetamide (**5**):* ^{1}H NMR (600 MHz, $CDCl_3$) δ 7.69 (s, 1H), 7.59 (d, J = 9 Hz, 2H), 7.40 (d, J = 8.5 Hz, 2H), 7.37 (d, J = 8.5 Hz, 1H), 7.25 (m, 4H), 7.19 (d, J = 8.5 Hz, 2H), 7.15 (s, 1H), 7.10 (d, J = 8 Hz, 2H), 6.93 (m, 4H), 6.81 (d, J = 8 Hz, 2H), 6.68 (d, J = 8 Hz, 2H), 6.41 (m, 0.9H), 6.02 (br s, 0.9H), 5.08 (s, 2H), 4.56 (m, 4H), 3.83 (s, 3H), 3.78 (s, 3H), 3.71 (s, 3H), 3.64 (dd, J = 15, 25 Hz, 2H), 3.56 (s, 1H). ^{13}C NMR (150 MHz, $CDCl_3$) δ 176.1, 173.4, 169.7, 159.5, 158.7, 158.6, 158.4, 157.3, 138.0, 134.2, 130.3, 130.0, 129.9, 129.8, 129.3, 129.2, 129.0, 128.8, 128.6, 128.5, 127.6, 127.5, 127.4, 127.3, 127.2, 126.6, 125.7, 119.6, 114.0, 113.9, 113.8, 106.7, 69.8, 63.4, 55.3, 55.2, 49.8, 43.6, 40.4, 40.0. ESI-TOF calcd for $C_{44}H_{42}N_2O_6$ [M + H$^+$] 695.3115, found 695.3092.

*N-Benzyl-2-[N-butyl-2-(4-methoxyphenyl)acetamido]-2-[6-(4-methoxybenzyloxy)naphthalen-2-yl]acetamide (**6**):* ^{1}H NMR (600 MHz, $CDCl_3$) δ 7.78 (s, 1H), 7.68 (dd, $J = 8.5$, 15 Hz, 2H), 7.41 (m, 3H), 7.22 (m, 10H), 6.95 (d, $J = 8.5$ Hz, 2H), 6.83 (d, $J = 8$ Hz, 2H), 6.54 (m, 0.8H), 6.00 (s, 0.9H), 5.10 (s, 2H), 4.46 (ddd, $J = 5.5$, 15, 34 Hz, 2H), 3.83 (s, 3H), 3.78 (s, 3H), 3.73 (dd, $J = 15$, 20 Hz, 2H), 3.35 (m, 2H), 1.41 (m, 1H), 1.04 (m, 3H), 0.67 (t, $J = 7$ Hz, 3H). ^{13}C NMR (150 MHz, $CDCl_3$) δ 172.4, 170.0, 159.5, 158.5, 157.4, 138.1, 134.2, 130.5, 130.3, 129.9, 129.6, 129.3, 128.6, 128.5, 128.4, 127.6, 127.4, 127.3, 126.9, 119.6, 114.4, 114.1, 114.0, 106.8, 103.0, 69.8, 63.0, 55.3, 55.2, 47.2, 43.6, 40.0, 31.8, 20.0, 13.4. ESI-TOF calcd for $C_{40}H_{42}N_2O_5$ [M + H$^+$] 631.3166, found 631.3145.

*2-(6-Benzyloxynaphthalen-2-yl)-N-cyclohexyl-2-{(2-methoxyethyl)-[2-(4-methoxyphenyl)acetyl]amino}acetamide (**7**):* ^{1}H NMR (600 MHz, $CDCl_3$) δ 7.79 (m, 1H), 7.70 (t, $J = 8$ Hz, 1H), 7.65 (dd, $J = 3$, 8 Hz, 1H), 7.49 (m, 2H), 7.38 (m, 4H), 7.22 (m, 4H), 6.88 (dd, $J = 8$, 20.5 Hz, 2H), 6.16 (br d, $J = 8.5$ Hz, 0.5H), 5.99 (s, 0.6H), 5.72 (s, 0.4H), 5.29 (s, 0.5H), 5.17 (m, 2H), 3.82 (m, 6H), 3.61 (m, 05H), 3.43 (m, 1H), 3.31 (m, 1.5H), 3.14 (m, 3H), 1.93 (m, 2H), 1.78 (m, 1H), 1.66 (m, 2H), 1.58 (m, 1H), 1.37 (m, 2H), 1.13 (m, 3H). ^{13}C NMR (150 MHz, $CDCl_3$) δ 173.5, 168.9, 168.7, 158.6, 158.4, 157.3, 136.6, 134.1, 130.5, 130.0, 129.7, 128.9, 128.7, 128.6, 128.4, 128.1, 127.5, 127.3, 127.1, 126.5, 119.6, 114.2, 114.0, 106.9, 103.0, 70.9, 70.0, 69.6, 66.4, 62.9, 58.8, 58.4, 55.2, 48.6, 48.4, 41.0, 40.0, 33.3, 33.1, 32.8, 25.5, 25.4, 25.1, 24.8, 24.7. ESI-TOF calcd for $C_{37}H_{42}N_2O_5$ [M + H$^+$] 595.3166, found 595.3155.

N-{[6-(4-Methoxybenzyloxy)naphthalen-2-yl]methyl}propan-1-amine. *n*-Propylamine (21 μL, 260 μmol) was added to a solution of 6-(4-methoxybenzyloxy)-2-naphthaldehyde (50 mg, 170 μmol) in MeOH (1.36 mL). After being stirred at room temperature for 1 h, the solution was treated with AcOH (340 μL) and $NaBH_3CN$ (32 mg, 510 μmol). Once the reaction was deemed complete by TLC analysis (40% EtOAc/hexanes, 0.1% Et_3N), the unreacted $NaBH_3CN$ was quenched with 2 N HCl. The solution was filtered, and the solids were washed with water and then dried in vacuo to afford the product as a white solid (85%): ^{1}H NMR (400 MHz, DMSO-d_6) δ 9.23 (br s, 2H), 7.97 (s, 1H), 7.85 (t, $J = 7.5$ Hz, 2H), 7.65 (d, $J = 8.5$, 1H), 7.47 (d, $J = 2.5$ Hz, 1H), 7.44 (d, $J = 8.5$ Hz, 2H), 7.26 (dd, $J = 9$ Hz, 2.5 Hz, 1H), 6.97 (d, $J = 8.5$ Hz, 2H), 5.14 (s, 2H), 3.76 (s, 3H), 2.85 (br s, 2H), 1.68 (st, $J = 7.5$ Hz, 2H), 0.90 (t, $J = 7.5$ Hz, 3H). ^{13}C NMR (125 MHz, DMSO-d_6) 159.1, 156.9, 134.2, 129.7, 129.4, 129.3, 128.6, 127.9, 127.8, 127.1, 127.0, 119.5, 113.8, 107.2, 69.1, 55.0, 49.9, 47.9, 18.9, 11.0. ESI-TOF calcd for $C_{22}H_{25}NO_2$ [M + H$^+$] 336.1958, found 336.1973.

Docking Procedures. Docking calculations were performed using AutoDock 3.0.5. Amber-based "Kollman" partial atomic charges and solvation parameters were applied to atoms using the AutoDockTools software package. Energy grids for docking were generated by the program AutoGrid based on the acetylcholine esterase PDB entry 1J07. For the initial energy grids, ligand and water atoms were removed from the protein structure prior to AutoGrid calculations. In subsequent protein models, a few manually selected crystallographic waters within the peripheral active site region of AChE were retained for AutoGrid. No proton atoms were added to the crystallographic water molecules. The energy grids were 70 Å $\times$ 50 Å $\times$ 70 Å in dimension with a 0.375 Å grid spacing and were centered on the propidium crystallographic position. Chemical structures were generated by creating two-dimensional sdf files with ChemDraw and converting these files into three-dimensional structures using INSIGHT. Ligand pdbq files for use in AutoDock were generated using AutoDockTools commands from a Python script. Gasteiger charges were assigned to ligand atoms. For each ligand, an AutoDock calculation consisted of eight separate docking calculations. Each docking calculation consisted of 1×10^8 docking evaluations using the Lamarckian genetic algorithm−local search (GALS) method (*19*). The GALS method is an evolutionary algorithm that evaluates a population of possible docking solutions and propagates the most successful individuals from each generation into the subsequent generation of possible solutions. A low-frequency local search method according to the method of Solis and Wets is applied to docking solutions to ensure the final solution represents the local minima. All dockings were performed with a generation population size of 200 and 300 rounds. Solis and Wets local searches were applied with a probability of 6%. A crossover rate of 80% was used to generate new docking solutions for subsequent generations, and one solution from each generation was propagated to the next generation. Each of the eight docking solutions were clustered on the basis of the root mean square deviation (RMSD) between the Cartesian coordinates of the atoms and ranked on the basis of free energy of binding. For the credit card library, the docking energy results for all eight docking calculations for every compound were compiled into a docking energy list and sorted by lowest docking energy. The lowest docking energy conformation for each compound was used to seed a new AutoDock calculation. This procedure was repeated until the order of the compounds in the docking energy list was consistent from round to round. The order of compounds in the docking energy list became consistent after the third round, but five rounds were calculated in total to ensure convergence of the docking results.

Acetylcholinesterase Inhibition Studies. All assays were preformed using a Cary 50 Bio UV−visible spectrophotometer using an 18-cell changer and conducted at 37 °C, using a Cary PCB 150 water peltier system. Solutions of acetylthiocholine iodide (ATCh iodide) and 5,5′-dithiobis(2-nitrobenzoic acid) (DTNB) were prepared according to the method published by Ellman et al. (*20*). Stock solutions of acetylcholinesterase from *E. electricus* were prepared by dissolving commercially available enzyme in 1% gelatin. Prior to use, an aliquot of the gelatin solution was diluted 1:200 in water. For the assay, the solution was diluted until enzyme activity between 0.1 and 0.13 AU/min at 500 μM ACTh iodide was obtained. Compounds were prepared as solutions in methanol.

Assays were performed by mixing AChE, test compound, and 340 μM DTNB in 100 mM phosphate buffer, pH 8.0, containing 5% methanol. Solutions were incubated at 37 °C for 5 min before the reaction was initiated by the addition of ATCh iodide (75−300 μM). The increase of absorbance at 412 nm was monitored for 2−5 min. All assays were run in triplicate. Initial rates were determined by subtracting the average observed initial rate from the nonenzymatic reaction.

For each tested compound, linear regression analysis of reciprocal plots of $1/v_0$ versus 1/[S] for four test compound concentrations was preformed using Microsoft Excel software. The $\text{slope}_{1/v}$ was plotted against [I] to give K_i values. Propagation of error was preformed to determine the error, ΔK_i.

AChE-Induced β-Amyloid Peptide Aggregation in the Presence of AChE Ligands. The aggregation of the β-amyloid peptide was measured using the thioflavin T-based fluorometric assay as described by LeVine (*21*) and Bartolini (*14*). Assays were measured using a SpectraMAX Gemini fluorescence plate reader with SOFTmax PRO 2.6.1 software. $A\beta_{1-40}$ stock solutions were prepared in DMSO, and HuAChE stocks were prepared in distilled water. All stock solutions of Aβ and HuAChE were used immediately after preparation.

In a 96-well plate, triplicate samples of a 20 μL solution of 23 nM Aβ, 2.30 μM HuAChE, and various concentrations of test compounds in 0.215 M sodium phosphate buffer, pH 8.0, were prepared. These solutions were incubated at room temperature along with triplicate solutions of Aβ alone, Aβ and AChE, and Aβ plus test compounds at various concentrations. After 48 h, a 2 μL aliquot was removed from each well, placed in a black-walled, clear-bottomed 96-well plate, and diluted with 50 mM glycine−NaOH buffer, pH 8.5, containing 1.5 μM thioflavin T to a total volume of 200 μL. After incubation for 5 min, the fluorescence was measured using $\lambda_{exc} = 466$ nm and $\lambda_{em} = 490$ nm with excitation and emission slits of 2 nm. The fluorescence emission spectrum was recorded between 450 and 600 nm, with excitation at 446 nm.

The fluorescence intensities were averaged, and the average background fluorescence of buffer only, or buffer and test compound, was subtracted. The corrected fluorescence values were plotted with their standard deviation. The equation $F_i/F_0 \times 100\%$, where F_i is the fluorescence of AChE, Aβ, and test compound and F_0 is the fluorescence of AChE and Aβ, was used to quantify the extent to which each compound inhibits Aβ aggregation.

Butyrylcholinesterase Inhibition Studies. Butyrylcholinesterase (BuChE) from equine serum was prepared and assayed as described for AChE save that assays were conducted in a Molecular Devices Corp. Spectra Max 250 microtiter plate reader, and IC_{50} values were determined using 125 μM ATCh iodide.

Fluorogenic Ligand Displacement Measurements. The affinity of **3** for the peripheral binding site of AChE was determined through the displacement of propidium iodide using the method of Taylor et al. (*22*) as modified by Dodds and Rivory (*23*). Fluorescence titrations were conducted in 1 mM Tris, pH 8.0, at 25 °C with a 10-fold excess of propidium iodide over enzyme. Stocks of propidium iodide and compound **3** were prepared in methanol. Assays were conducted using a thermostated ISA FluoroMax-2 spectrofluorometer. Displacement titrations were performed using enzyme concentrations of 1.2, 0.60, and 0.225 μM. Under conditions where the concentration of enzyme approaches the K_d of a compound, the standard approximation of $[I]_{free} = [I]_{total}$ is incorrect. Instead, the system is considered to be under tight binding conditions, and the full expression for free inhibitor is required as described by Morrison (*24*). To get a more accurate determination of K_d under tight binding conditions, the concentration of enzyme was varied (*25*) and titrations were fit simultaneously to

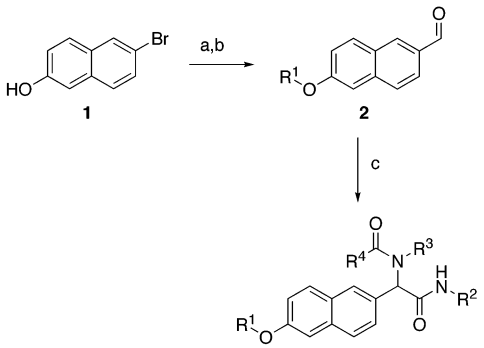

FIGURE 1: Synthesis of credit card library members using the Ugi reaction. Reagents: (a) *n*-BuLi (2 equiv), THF, −78 °C, then DMF; (b) R^1Br, K_2CO_3, DMF, 80 °C; (c) R^2NC, R^3NH_2, R^4CO_2H, MeOH/$CHCl_3$, reflux.

$$F = F_1\left(1 - \frac{[EI]}{E_T}\right) + F_0 \quad (1)$$

$$[EI] = \frac{E_T + I_T + K_d - \sqrt{(E_T + I_T + K_d)^2 - 4E_TI_T}}{2} \quad (2)$$

where F, F_1, and F_0 are the observed fluorescence, the fluorescence of AChE-bound propidium, and the fluorescence at ligand saturation, respectively. E_T, I_T, and K_d are the total enzyme present, total ligand present, and the dissociation constant for the enzyme−ligand complex, respectively. Simultaneous nonlinear least-squares fitting of the three titrations was performed with MacCurveFit (Kevin Raner Software).

RESULTS AND DISCUSSION

The use of small molecules and peptides as inhibitors of Aβ oligomerization has become increasingly popular as a promising pharmacotherapy for AD. However, assaying libraries for inhibition of Aβ aggregation can be a very expensive endeavor in light of the large quantities of enzyme and peptide needed for screening. Even with small focused libraries such as the one employed in this study, the cost of Aβ and human AChE can rapidly escalate into the tens of thousands of dollars, well beyond the financial means of most academic laboratories. Consequently, we turned to in silico docking methodology as a means to guide our experimental screens (*26*).

The design principle of our library is based upon a planar naphthalene core credit card structure with appended α-acylamino amide diversity introduced through the Ugi four-component condensation (4CC) reaction (*27*). Thus, our initial design strategy was aimed at interrupting the Aβ−AChE PAS protein−protein interaction without specific regard for recognition of the enzyme active site. Represented among library members are diversity elements with a wide range of size, polarity, aromaticity, and hydrogen-bonding capability. The synthesis of each compound was performed in two or three steps (Figure 1). Lithiation of 6-bromo-2-naphthol (**1**) and quenching with DMF yielded general building block 6-hydroxy-2-naphthaldehyde (**2**), which was then treated with various alkyl halides to generate the

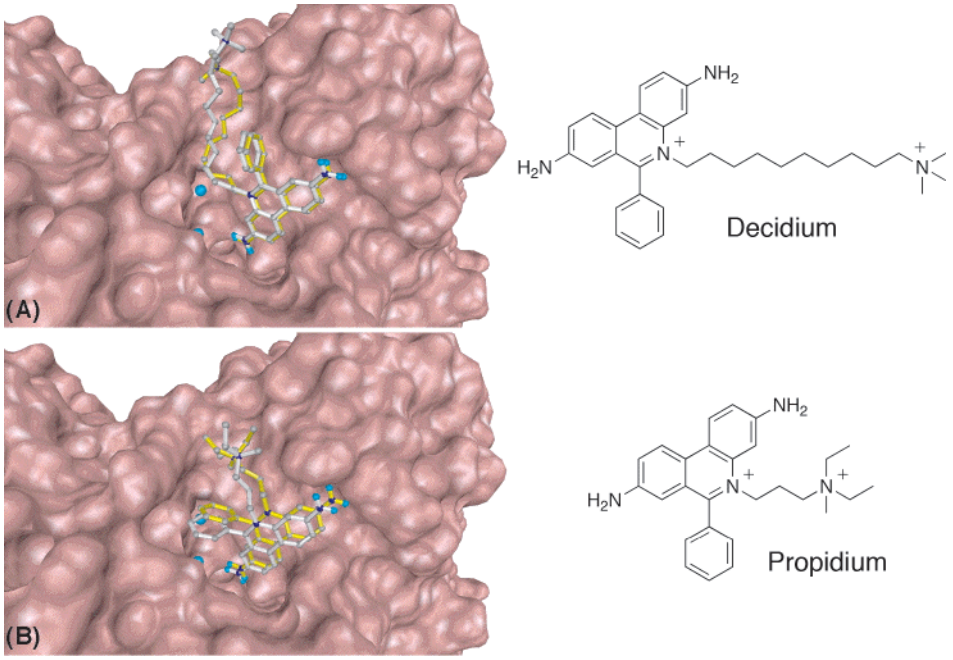

FIGURE 2: (a) Decidium and (b) propidium docking results (yellow) compared with crystallographic results (gray).

corresponding phenolic ethers, the starting material for our Ugi reactions. Using a combination of naphthals, isocyanides, amines, and carboxylic acids, the desired Ugi condensation products were obtained in acceptable yields and high purities (>95%) after chromatographic purification. The total library was composed of 271 members, and for the purposes of these studies, all compounds were prepared in racemic form. While we acknowledge that it is likely that one enantiomer is more active than the other, the preparation of enantiopure Ugi reaction products is cumbersome and not readily amenable to the rapid synthetic time scale needed for efficient library preparation.

The crystal structure of mouse acetylcholinesterase (mAChE) with the inhibitor decidium bound at the PAS was used for docking studies with the program AutoDock 3.0.5 (*19*). For the initial protein model, all crystallographic waters and other ligands save for two chloride ions were removed from the crystal structure, and the resulting structure was used to generate energy maps with AutoGrid. The energy grid included both the PAS region and the central binding gorge containing the active site catalytic triad. Thus the AutoDock calculations considered the possibility of binding to either, or both, sites. As an initial test of the accuracy of AutoDock with this protein model, the docking results for the PAS inhibitors propidium were compared to the mAChE−propidium crystal structure. Unfortunately, this initial docking model did not accurately reproduce the literature crystallographic results; the RMS difference between the predicted and the crystallographic ligand position was 4.9 Å. It was observed that while the docked propidium binds in the PAS, the docked position is rotated approximately 90° from the crystallographic position (data not shown).

To improve the accuracy of the docking calculations, two crystallographic waters within 3 Å of the decidium molecule were added to the docking model. Both of these waters are strongly bound to the enzyme by multiple backbone hydrogen bonds and thus are expected to be rigid relative to bulk water. Furthermore, we anticipated that these water molecules would enhance ligand recognition in the PAS as well as occlude a portion of the binding site near Phe295 and Arg296. The two-water mAChE docking model resulted in docking predictions that were more similar to the crystallographic complexes (RMSD 1.8 Å for propidium, 1.5 Å for decidium). Examination of the model revealed that the decidium docking prediction shows excellent agreement with the crystallographic position at the fused ring portion of the molecule, while the acyl tail of the decidium shows some deviation from the crystal structure (Figure 2). In contrast, the propidium docking prediction is accurately positioned but is offset slightly from the actual position as reported in the crystal structure (Figure 2).

On the basis of the success of the docking experiments using previously characterized PAS inhibitors, the 271 compounds from the Ugi condensation product library were docked to the two-water mAChE energy maps. The predicted binding energies from these compounds ranged from −11.2 to −4.7 kcal/mol, with a mean value and standard deviation of −7.7 and 1.1 kcal/mol, respectively. Unfortunately, the top scoring compound was predicted to bind within the mAChE active site rather than the PAS and was excluded from further studies. However, on the basis of this model most of the compounds were predicted to bind in the PAS. The second ranked compound in terms of binding energy bound in the PAS with a predicted binding energy of −10.84 kcal/mol. Forty-six compounds had predicted binding energies that were within the AutoDock standard error of 2.0 kcal/mol to the highest ranked PAS binder. By comparison, the docking energies for propidium and decidium were −8.3 and −8.5 kcal/mol, respectively. Surprisingly, analysis of the docking results for the entire library revealed that 63 of the 271 compounds (23% of the library) had a higher predicted docking energy than propidium and decidium, suggesting that a large fraction of the compound library could be potent inhibitors of amyloid formation.

Although the docking studies showed that a large percentage of the library bound to the AChE PAS with comparable

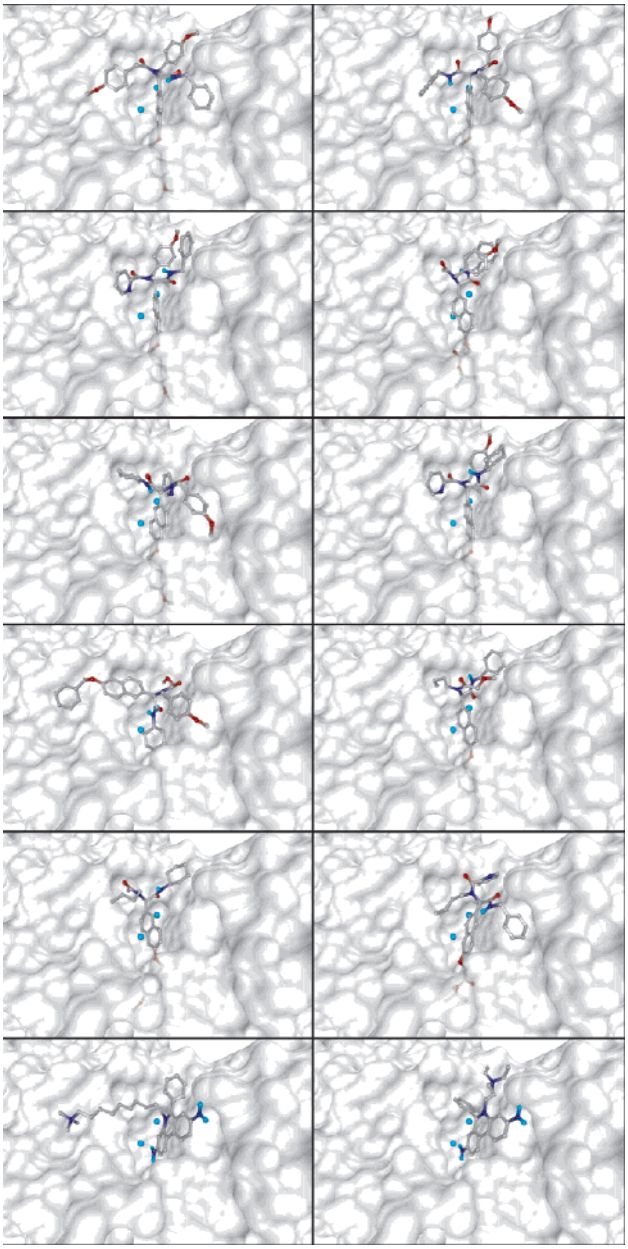

FIGURE 3: Ten best compounds from the credit card library in order of predicted binding energy from left to right. For comparison, decidium and propidium structures are shown in the bottom two panels.

affinity to propidium, only the 10 compounds with the highest predicted binding energies were examined in further experiments. Comparison of the structures of these compounds revealed some general trends regarding the nature of PAS binding compounds. The AutoDock results favor the bulkier compounds with aromatic groups, particularly *p*-methoxybenzyl at the R^1 position, benzyl at the R^2 position, benzyl ethers at R^3, and *p*-methoxybenzyl ethers at the R^4 position (Figure 3).

On the basis of the docking results, almost all of the library members are predicted to bind in approximately the same position in the PAS, and in particular, the naphthalene core and R^1 side chain positions are well conserved. The naphthyl portion is most often found to pack against the Trp286 indole side chain. The R^1 side chain binds in the protein tunnel leading to the catalytic triad active site in most of the docking predictions. This tunnel is flanked by four tyrosines (residues 72, 124, 337, and 341), which interact with the R^1 side chain. For most of the library members, the R^1 side chain has significantly higher predicted van der Waals energies than the other side chains. AutoDock predicts binding pockets for the other three points of diversity (R^2, R^3, and R^4). The central binding pocket (P1) for the compounds in the PAS is formed by residues 288−298, which form a turn at the end of an α-helix. Two superficial binding pockets flank the central binding pocket on either side. The second binding pocket (P2) is formed between Glu292 and the backbone of residues 341 and 342. The third binding pocket (P3) is formed between His287 and Tyr72. Each of these three pockets is predicted to have affinity for aromatic compounds, but there does not appear to be a preference for a particular side chain position (R^2, R^3, or R^4) at any of these pockets. For example, in the case of the highest ranked compound, the R^4 pyridyl moiety fits in the P1 pocket, the R^2 cyclohexyl group in the P2 pocket, and the R^3 *p*-methoxybenzyl group to the P3 pocket. Hydrogen bonds are formed to the compound's R^4 scaffold carbonyl by His287 and to the R^1 ether oxygen by Asn87 (Figure 3). In contrast, examining the docking results of the next ranked compound in terms of binding energy revealed that both the R^2 phenyl and R^3 *p*-methoxybenzyl groups fit into the P1 pocket, while the R^4 pyridyl group is positioned in the P2 pocket (Figure 3). Hydrogen bonds may be formed to the R^4 pyridine nitrogen by the Tyr341 carbonyl and also to the R^1 ether oxygen by Asn87. Thus, although the orientation of the naphthalene core appears to be fairly conserved across the most promising compounds, there is considerable variability in the positioning of the other moieties, resulting in differences in binding energy.

With the information derived from AutoDock calculations, the 10 compounds with highest predicted affinity were screened in vitro using Ellman's colorimetric assay (*20*). While all 10 compounds displayed some AChE inhibition, only compounds that achieved ≥50% inhibition from an initial screen using 5 μM test compound and 175 μM ATCh iodide were advanced into further kinetic analysis. The five compounds that satisfied this criterion (Figure 4) were all low micromolar inhibitors of AChE activity and displayed linear double reciprocal Lineweaver−Burk plots consistent with competitive inhibition of AChE (Figure 5). Replots of the slope of the Lineweaver−Burk plot versus compound concentration were also linear and returned values for K_i ranging from 1.9 to 14.2 μM (Table 1). While this level of inhibition is modest compared to other characterized AChE inhibitors, the determined K_i values are comparable to previously identified compounds that display tight binding with the AChE PAS (e.g., propidium) (*26*, *28*). Interestingly, despite the variability observed in the orientation of the best compounds in the docking studies, lead compounds retained significant homology between the substituents (Figure 4). To assess if the core structure itself could serve as an inhibitor, a control compound was synthesized and evaluated for AChE inhibition (Figure 6). Gratifyingly, no inhibition was observed under the assay conditions, suggesting that the observed inhibitory activity is not simply a function of the naphthalene core structure.

While most PAS ligands of AChE display either noncompetitive or mixed-type inhibition, competitive inhibition was expected for the credit card compounds on the basis of the

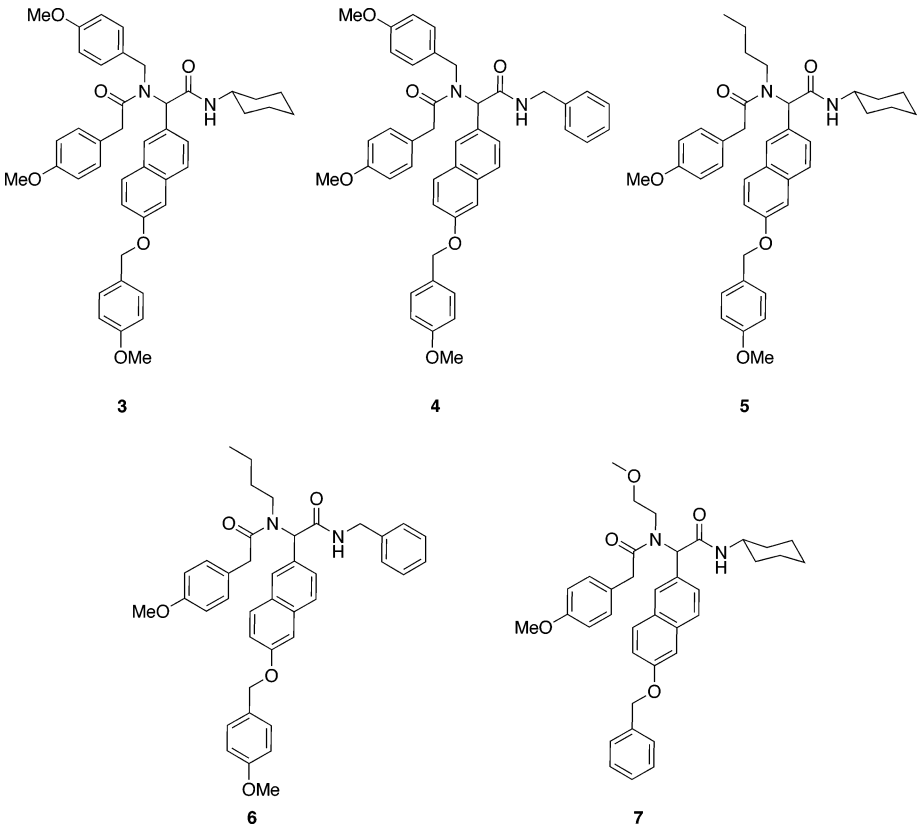

FIGURE 4: Chemical structures of five lead compounds displaying at least 50% inhibition of AChE under the stated screening conditions.

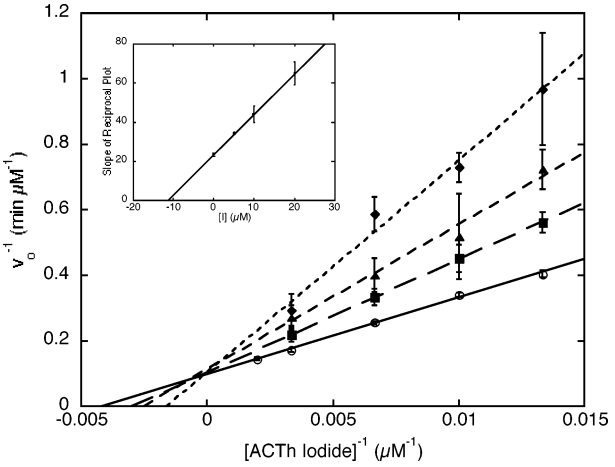

FIGURE 5: Steady-state competitive inhibition of AChE by credit card compounds. Reciprocal plots of initial velocity and substrate concentration (75−300 μM) are shown. Inset: Replot of slope versus inhibitor concentration for the determination of K_i. As a representative example, compound **5** is shown.

AutoDock calculations, which predicted that the R^1 side chain binds to AChE in the channel leading to the catalytic triad active site, thus precluding the formation of an ESI complex. Further kinetic evidence for the AutoDock predictions was obtained by determining the mutual exclusivity of **3**, a purely competitive inhibitor, and propidium, a well-characterized purely noncompetitive inhibitor. Dixon plots of initial rate versus concentration of **3** at fixed propidium concentrations returned a series of parallel lines (*29*), indicating that **3** and propidium cannot bind to AChE simultaneously and verifying the docking results that these compounds bind in the peripheral anionic site. In a parallel approach, we also examined the ability of **3** to affect PAS binding using a fluorogenic ligand displacement assay. As can be seen in Figure 7, **3** binds tightly to AChE in the low micromolar concentration range and displaces propidium completely. Simultaneous fitting to all three titration experiments predicts a K_d for this interaction of 0.3 ± 0.2 μM. This value is somewhat tighter than that predicted by kinetic analysis, but

Table 1: Activity of Compounds **3**−**7** against AChE (K_i) and Aβ Aggregation

entry	compound	K_i (μM)	% Aβ inhibition
1	**3**	1.9 ± 0.1	77 ± 4.3
2	**4**	6.9 ± 2.3	78 ± 4.5
3	**5**	11.5 ± 0.3	78 ± 6.7
4	**6**	14.2 ± 4.0	76 ± 4.6
5	**7**	10.2 ± 1.6	79 ± 3.5
6	propidium	13.5 ± 2.1	80 ± 0.4
7	tacrine[a]	0.15 ± 0.02	not active

[a] From ref *25*.

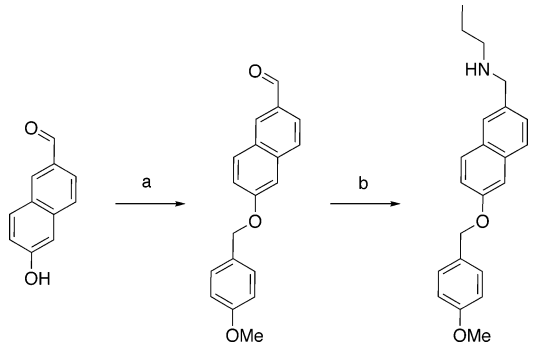

FIGURE 6: Synthesis of a control compound used to assess the potential of AChE inhibition by the credit card core. Reagents: (a) *p*-methoxybenzyl chloride, K_2CO_3, DMF, 80 °C; (b) *n*-propylamine, MeOH, 1 h, then $NaBH_3CN$, AcOH.

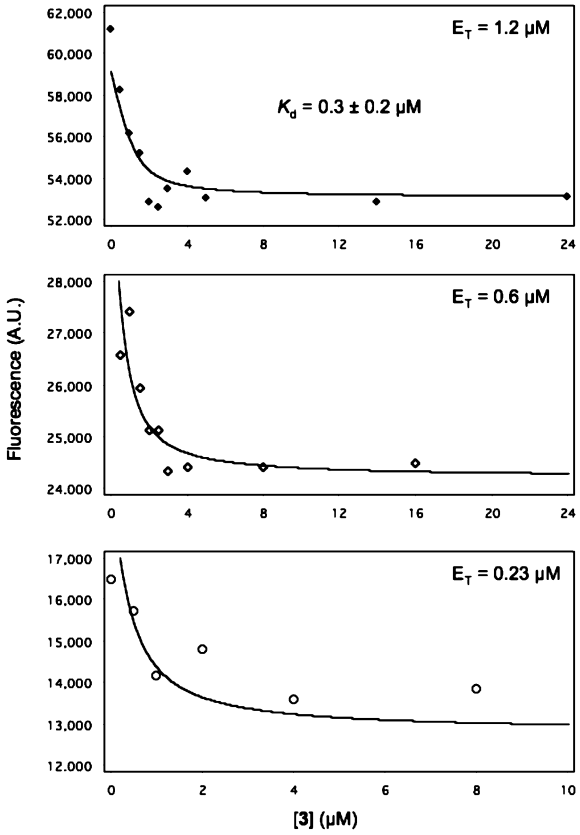

FIGURE 7: Simultaneous fit of the Morrison equation to propidium iodide displacement titrations at different enzyme concentraions.

consistent with tight binding to the peripheral site.

Given these positive results into the mode and potency of AChE inhibition, the five lead compounds were assayed for their ability to inhibit the ability of AChE to enhance Aβ aggregation. Using a thioflavin T-based fluorometric assay (*21*) the percent inhibition of amyloid fibril formation attributable to the selected compounds was determined. In this assay, the concentration of ligand used is significantly larger than the determined K_i values; however, this is necessary as higher AChE and Aβ concentrations are required in this assay to accelerate the aggregation process such that measurements can be made in a reasonable period of time (*14*). Using 100 μM test compound, all five of the tested compounds eliminated the portion of Aβ aggregation induced by AChE (Table 1). All compounds displayed a potency of inhibition, within error, to that of propidium, one of the most effective inhibitors of Aβ aggregation, and well beyond that of tacrine, a common PAS binder currently approved for the treatment of AD in humans (*13*, *14*, *30*). Tacrine is capable of treating cholinergic loss by potent inhibition of AChE and, thus, acetylcholine degradation; alternatively, our identified compounds address the noncatalytic role of AChE in AD, that is, the enhancement of Aβ aggregation. In conjunction with our AChE inhibition studies, these results provide parallel validation of the AutoDock model and give further evidence that the identified compounds bind to the same region of the PAS as propidium and thus serve as novel leads for the development of AD therapeutics.

Recent reports have suggested that the selectivity of a given inhibitor for AChE over butyrylcholinesterase (BuChE) could be correlated with the ability of a compound to block AChE-accelerated Aβ aggregation (*15*, *31*). Consequently, we examined the ability of our lead compounds to inhibit BuChE. However, within their limits of solubility (approximately 100 μM), **3**−**7** did not inhibit this enzyme, and no quantitative ratio could be determined. The observed selectivity of the target library for AChE over BuChE is consistent with a specificity for the PAS as this site is not present in BuChE (*32*), despite the known preference of the BuChE active site gorge for large lipophilic compounds (*33*).

We have reported an approach for the development of amyloid aggregation inhibitors using a combinatorial credit card concept combined with computational library screening as a method for identifying compounds that disrupt protein−protein interactions. Although the potential relevance of the described lead compounds in AD treatment is clear, our library design approach should also find use in biophysical studies focused on elucidating the critical structure determinants for a given protein−protein interaction. While further studies are required to assess the cytotoxicity of these lead compounds prior to advancement into more advanced disease models, our previous experiments using this library in other biological scenarios have demonstrated that many of these compounds are viable in mammalian cell-based assays with no apparent cytotoxicity (*18*). Critically, this study illustrates the power of rational library design in conjunction with in silico docking methods for focused screening efforts. Furthermore, our derived computational model for AChE PAS docking allows for the screening of large numbers of compounds at rates much greater than compound libraries can be prepared, purified, and characterized.

REFERENCES

1. Ritchie, K., and Kildea, D. (1990) Is senile dementia "age-related" or "ageing-related"? Evidence from meta-analysis of dementia prevalence in the oldest old. *Lancet 346*, 931−934.
2. Iqbal, K. (1991) *Prevalence and neurobiology of Alzheimer's disease*, John Wiley and Sons, New York.
3. Rozemuller, J. M., Eikelenboom, P., Stam, F. C., Beyreuther, K., and Master, C. L. (1989) A4 protein in Alzheimer's disease; primary and secondary cellular events in extracellular amyloid deposition, *J. Neuropathol. Exp. Neurol. 48*, 674−691.
4. Evans, D. A. (1990) Estimated prevalence of Alzheimer's disease in the United States, *Milbank Q. 68*, 267−289.
5. Wisniewski, H. M., Ghetti, B. H., and Terry, R. D. (1973) Neuritic (senile) plaques and filamentous changes in aged rhesus monkeys, *J. Neuropathol. Exp. Neurol. 32*, 566−584.
6. Itagaki, S., McGeer, P. L., Akiyama, H., Zhu, S., and Selkoe, D. (1989) Relationship of microglia and astrocytes to amyloid deposits of Alzheimer disease, *J. Neuroimmunol. 24*, 173−182.
7. Perlmutter, L. S., and Chui, H. C. (1990) Microangiopathy, the vascular basement membrane and Alzheimer's disease: a review, *Brain Res. Bull. 24*, 677−686.
8. Hardy, J., and Allsop, D. (1991) Amyloid deposition as the central event in the aetiology of Alzheimer's disease, *Trends Pharmacol. Sci. 12*, 383−388.
9. Hardy, J. A., and Higgins, G. A. (1992) Alzheimer's disease: the amyloid cascade hypothesis, *Science 256*, 184−185.
10. Bloom, G. S., Ren, K., and Glabe, C. G. (2005) Cultured cell and transgenic mouse models for tau pathology linked to β-amyloid, *Biochim. Biophys. Acta 1739*, 116−124.
11. Holcomb, L. A., Gordon, M. N., Benkovic, S. A., and Morgan, D. G. (2000) Aβ and perlecan in rat brain: glial activation, gradual clearance and limited neurotoxicity, *Mech. Aging Dev. 112*, 135−152.
12. Alvarez, A., Alarcon, R., Opazo, C., Campos, E. O., Munoz, F. J., Calderon, F. H., Dajas, F., Gentry, M. K., Docctor, B. P., De Mello, F. G., and Inestrosa, N. C. (1998) Stable complexes involving acetylcholinesterase and amyloid-β peptide change the

biochemical properties of the enzyme and increase the neurotoxicity of Alzheimer's fibrils, *J. Neurosci. 18*, 3213−3223.
13. Inestrosa, N. C., Alvarez, A., Perez, C. A., Moreno, R. D., Vicente, M., Linker, C., Casanueva, O. I., Soto, C., and Garrido, J. (1996) Acetylcholinesterase accelerates assembly of amyloid-β-peptides into Alzheimer's fibrils: possible role of the peripheral site of the enzyme, *Neuron 16*, 881−891.
14. Bartolini, M., Bertucci, C., Cavrini, V., and Andrisano, V. (2003) β-Amyloid aggregation induced by human acetylcholinesterase: inhibition studies, *Biochem. Pharmacol. 65*, 407−416.
15. Piazzi, L., Rampa, A., Bisi, A., Gobbi, S., Belluti, F., Cavalli, A., Bartolini, M., Andrisano, V., Valenti, P., and Recanatini, M. (2003) 3-(4-{[Benzyl(methyl)amino]methyl}-phenyl)-6,7-dimethoxy-2*H*-2-chromenone (AP2238) inhibits both acetylcholinesterase and acetylcholinesterase-induced β-amyloid aggregation: A dual function lead for Alzheimer's disease therapy, *J. Med. Chem. 46*, 2279−2282.
16. Rampa, A., Bisi, A., Belluti, F., Gobbi, S., Valenti, P., Andrisano, V., Cavrini, V., Cavalli, A., and Recanatini, M. (2000) Acetylcholinesterase inhibitors for potential use in Alzheimer's disease: Molecular modeling, synthesis and kinetic evaluation of 11*H*-indeno-[1,2-*b*]-quinolin-10-ylamine derivatives, *Bioorg. Med. Chem. 8*, 497−506.
17. Reyes, A. E., Perez, D. R., Alvarez, A., Garrido, J., Gentry, M. K., Doctor, B. P., and Inestrosa, N. C. (1997) A monoclonal antaibody against acetylcholinesterase inhibits the formation of amyloid fibrils induced by the enzyme, *Biochem. Biophys. Res. Commun. 232*, 652−655.
18. Yamamoto, N., Shi, J., Xu, Y., Vogt, P. K., and Janda, K. D. (2005) A credit card library approach for disrupting protein−protein interactions, *Chem. Biol.* (submitted for publication).
19. Morris, G. M., Goodsell, D. S., Halliday, R. S., Huey, R., Hart, W. E., Belew, R. K., and Olson, A. J. (1998) Automated docking using a Lamarckian genetic algorithm and empirical binding free energy function, *J. Comput. Chem. 19*, 1639−1662.
20. Ellman, G. L., Courtney, K. D., Andres, V., Jr., and Featherstone, R. M. (1961) A new and rapid colorimetric determination of acetylcholinesterase activity, *Biochem. Pharmacol. 7*, 88−95.
21. LeVine, H., III (1993) Thioflavine T interaction with synthetic Alzheimer's disease β-amyloid peptides: detection of amyloid aggregation in solution, *Protein Sci. 2*, 404−410.
22. Taylor, P., Lwebuga-Mukasa, J., Lappi, S., and Rademacher, J. (1974) Propidium−A fluorescence probe for a peripheral anionic site on acetylcholinesterase, *Mol. Pharmacol. 10*, 703−708.
23. Dodds, H. M., and Rivory, L. P. (1999) The mechanism for the inhibition of acetylcholinesterases by irinotecan (CPT-11), *Mol. Pharmacol. 56*, 1346−1353.
24. Morrison, J. F. (1969) Kinetics of the reversible inhibition of enzyme-catalysed reactions by tight-binding inhibitiors, *Biochim. Biophys. Acta 185*, 269−286.
25. Murphy, D. J. (2004) Determination of accurate K_i values for tight-binding enzyme inhibitors: an in silico study of experimental error and assay design, *Anal. Biochem. 327*, 61−67.
26. Cavalli, A., Bottegoni, G., Raco, C., De Vivo, M., and Recanatini, M. (2004) A computational study of the binding of propidium to the peripheral anionic site of human acetylcholinesterase, *J. Med. Chem. 47*, 3991−3999.
27. Domling, A., and Ugi, I. (2000) Multicomponent reactions with isocyanides, *Angew. Chem., Int. Ed. 39*, 3169−3210.
28. Mizutani, M. Y., and Itai, A. (2004) Efficient method for high-throughput virtual screening based on flexible docking: Discovery of novel acetylcholinesterase inhibitors, *J. Med. Chem. 47*, 4818−4828.
29. Segel, I. H. (1975) *Enzyme Kinetics. Behavior and Analysis of Rapid Equilibrium and Steady-State Systems*, pp 474−479, John Wiley and Sons, New York.
30. Bolognesi, M. L., Andrisano, V., Bartolini, M., Banzi, R., and Melchiorre, C. (2005) Propidium-based polyamine ligands as potent inhibitors of acetylcholinesterase and acetylcholinesterase-induced amyloid β-aggregation, *J. Med. Chem. 48*, 24−27.
31. Belluti, F., Rampa, A., Piazzi, L., Bisi, A., Gobbi, S., Bartolini, M., Andrisano, V., Cavalli, A., Recanatini, M., and Valenti, P. (2005) Cholinesterase inhibitors: Xanthostigmine derivatives blocking the acetylcholinesterase-induced β-amyloid aggregation, *J. Med. Chem. 48*, 4444−4456.
32. Massoulie, J., Sussman, J., Bon, S., and Silman, I. (1993) Structure and functions of acetylcholinesterase and butyrylcholinesterase, *Prog. Brain Res. 98*, 139−146.
33. Rampa, A., Piazzi, L., Belluti, F., Gobbi, S., Bisi, A., Bartolini, M., Andrisano, V., Cavrini, V., Cavalli, A., Recanatini, M., and Valenti, P. (2001) Acetylcholinesterase inhibitors: SAR and kinetic studies on omega-[*N*-methyl-*N*-(3-alkylcarbamoyloxyphenyl)methyl]aminoalkoxyaryl derivatives, *J. Med. Chem. 44*, 3810−3820.

BI051613X